A_1(LO) phonon structure in degenerate InN semiconductor films

J. S. Thakur,[1,*] D. Haddad,[2] V. M. Naik,[3] R. Naik,[2] G. W. Auner,[1] H. Lu,[4] and W. J. Schaff[4]
[1]*Department of Electrical and Computer Engineering, Wayne State University, Detroit, Michigan 48202, USA*
[2]*Department of Physics and Astronomy, Wayne State University, Detroit, Michigan 48202, USA*
[3]*Department of Natural Sciences, University of Michigan-Dearborn, Dearborn, Michigan 48128, USA*
[4]*Department of Electrical and Computer Engineering, Cornell University, Ithaca, New York 14583, USA*
(Received 17 September 2004; published 9 March 2005)

We have studied the A_1(LO) structure of InN thin films from a low (n_e=6.7×10^{17}/cm^3) to a very high (n_e=9.6×10^{20}/cm^3) carrier concentration using Raman scattering experiments. Theoretically we investigated this structure using a wave vector **q** dependent dielectric function $\varepsilon(q,\omega)$ which takes into account the coupling of longitudinal-optical (LO) phonon and degenerate electrons with nonparabolic energy dispersion. Interaction of the phonon and undamped wave-vector-dependent plasmon yields two coupled modes with energies much different from the observed structure and thus cannot explain the origin of this structure. However, phonon interaction with electron-hole pair excitations forms a well-defined structure in Im $\varepsilon(q,\omega)^{-1}$ which begins to emerge at smaller values of **q** from the electron-hole pairs spectrum when the higher-energy coupled mode becomes Landau damped. With increasing values of **q**, the peak position of this structure moves towards the experimental value. This peak structure is formed by a comparatively weaker (relative to the plasmon) interaction between the LO-phonon and electron-hole pair excitations. Experimentally it is observed that the energy of this structure increases with increasing value of electron density.

DOI: 10.1103/PhysRevB.71.115203 PACS number(s): 63.20.−e, 78.30.−j, 78.66.Fd

I. INTRODUCTION

Recently, InN semiconductors have become a focus for extensive investigation of its optical[1–5] and electrical properties[6,7] because of their potential applications in laser diodes, high-temperature, and high-power electronic devices. The band gap, the most important physical property, of the InN semiconductor films has been under intense reinvestigation due to the controversy in the experimentally observed values which vary over a large range from 0.6 eV (Refs. 1,3) to 1.9 eV (Ref. 8) and in the origin of its variation.[9–11] Most of the measurements that have been made provide direct qualitative and quantitative estimates of various physical parameters[12] of the system, which are required for device characterization. The elementary excitations of the system play an important role in these measurements, leading to their extensive investigation using both theoretical[13–17] and experimental techniques.[18,19]

The behavior of the LO-phonon excitations in these materials is particularly intriguing because of their Frõhlich interaction[20] with conduction-band electrons, which also makes its experimental observation[18,19] and interpretation more difficult and challenging. However, many experiments reveal a well-defined structure whose energy varies[21,22] from 574 cm^{-1} to 596 cm^{-1} and so far the origin of this wide variation in the energy is not very well understood yet. These values, however, match with the theoretically calculated energy of the LO phonon[15–17] and therefore this structure has been directly identified with the excitation of the LO-phonon mode. In principle, the coupling of plasmon and LO-phonon mode should create two coupled modes with energies quite different from the fundamental modes (provided none of the fundamental modes is heavily damped) and suppress the unscreened LO phonon. So the origin of this structure and its association with the LO phonon (unscreened) is still not clear, although it has been observed in a wide variety of InN films with different thickness.[2,19] It is also not an artifact of the disorder in the film because this feature is observed in films with different mobility and phonon damping. On the other hand, if plasmon are strongly damped, then it can ruin the LO-phonon–plasmon mode interaction. In that case, the observed structure could be the unscreened LO phonon of the system.

Another important feature of this LO-phonon-like structure is that it has been observed in films with a wide range of carrier densities,[23,24] where the plasmon mode energy shows a significant variation. This suggests that the observed structure does not arise from any of the coupled modes due to the interaction of the long-wavelength ($\mathbf{q}\rightarrow 0$) plasmon and LO phonon, which are dependent on carrier density.

The LO-phonon-like structure of the InN materials is completely generic and also seems to be independent of the geometry of the films. It is true that a sufficiently deep-charge-depleted region (depletion width $W \geqslant 10$ nm) on the film surface or at the surface-substrate interface may lead to the emergence of the unscreened LO phonon in InN semiconductors. But even in films of smaller depletion regions[2] ($W \approx 5$ nm) this LO-phonon-like structure has been also observed. Moreover the characteristic resonant peak found in degenerate semiconductors due to the band gap transition can also not account for this structure as the latter's energy is much smaller than the direct-band value ($E_g \approx 0.70$ eV).[1,9,10]

One of the common features of this structure is a structural asymmetry, which for a purely collective excitation should be absent, as observed for the E_2 mode at 490 cm^{-1} of InN films. Asymmetry is a signature of the quantum interference[25,26] due to the overlap of discrete and continuum states. In degenerate semiconductors, continuum states are created when a finite momentum, delivered to the electronic subsystem, excites a number of electron-hole pairs (EHPs).

 ©2005 The American Physical Society

The macroscopic electric field associated with charge separation of these excitations interacts with the LO phonon and thus distorts the spectral symmetry of the mode. Transfer of momentum to the electronic subsystem can arise from various dynamical processes in the films. Elastic electron scattering, which is inevitable in these systems, may provide a significant momentum transfer to the electronic subsystem[28] and thus can modify the spectral features of the optical spectrum. Collisional damping of the electrons from randomly distributed ionized and other impurities can also produce nontrivial effects in the spectral line shapes.[27] The electron relaxation due to scattering from the LO phonon may lead to a momentum transfer q_{ep} of the order of $q_{ep} \approx \sqrt{2m_e^* \omega_{LO} \hbar^{-1}}$ which varies from $3 \times 10^6\ \mathrm{cm}^{-1}$ to $7 \times 10^6\ \mathrm{cm}^{-1}$ when the electron density increases from 6.7×10^{17} to $9.6 \times 10^{20}/\mathrm{cm}^3$. Here, m_e^* is the effective mass of the electron and ω_{LO} is the LO-phonon energy of InN semiconductors. For films with carrier densities $n_e \leqslant 3 \times 10^{19}/\mathrm{cm}^3$, the value of q_{ep} is larger than the plasmon cutoff wave vector. So in such cases there is a possibility that plasmon could be fully damped, and then the optical spectrum is determined by the weaker interaction between the LO-phonon and EHPs excitations rather than by the phonon plasmon mode interaction.

Experimental observations of symmetry-forbidden modes in the InN films also suggest a violation of momentum conservation in these systems. In the backscattering configuration $z(x,\cdot)\bar{z}$, for example, only E_2 and A_1(LO) modes are allowed by symmetry, but a significant intensity of A_1(TO)—a symmetry-forbidden mode—has been invariably observed in these experiments.[23,24] A symmetry-forbidden excitation can show up due to the presence of a large disorder in the samples, from internal reflection at the interfaces, and also from misalignment of the crystal symmetry axis with the probing axis in experimental settings, which is always difficult to overcome. Opaqueness of InN semiconductors can also account for the (inelastic) absorption of a large wave vector of the incident and scattered photons. The scattered wave vectors in this case are no longer real but complex[29] and the momentum absorbed by the system can be estimated from the optical absorption coefficient of the film.

II. EXPERIMENT

We investigated InN samples over a wide range of carrier density where the plasmon energy ω_p varies from $\omega_p \ll \omega_{LO}$ to $\omega_p \gg \omega_{LO}$. The InN films used in this study were grown at $\sim 470\ ^\circ\mathrm{C}$ by molecular beam epitaxy (MBE) at Cornell University[11] and by Plasma Source Molecular Beam Epitaxy (PSMBE) at Wayne State University (WSU).[10] Both the WSU and MBE samples were grown on *c*-plane sapphire substrates except in MBE samples there is an additional buffer layer structure consisting of ~200-nm-thick GaN on 10-nm-thick AlN. The MBE-grown samples were 0.6–2 μm thick with electron mobilities ranging from ~900 to $1300\ \mathrm{cm}^2/(\mathrm{V\ s})$, and were of lower carrier concentration ($n_e < 10^{19}\ \mathrm{cm}^{-3}$) compared to the WSU samples where $n_e > 10^{20}\ \mathrm{cm}^{-3}$ and electron mobilities $\sim 15\text{–}100\ \mathrm{cm}^2/(\mathrm{V\ s})$. Films grown at WSU are comparatively thinner having thickness ~0.5 μm. The optical absorption edge of MBE samples was 0.6–0.7 eV, whereas in the PSMBE samples it ranged from 1.5 eV to 1.9 eV. The variation of optical absorption edge in PSMBE samples is attributed to high electron degeneracy in the samples where a carrier-concentration-dependent Moss-Burstein shift leads to the higher values of the optical absorption edge.[10]

We have investigated the influence of different excitation energy on the Raman spectra of the films where the conduction-band electron density varies over a very wide range—$n_e = 6.7 \times 10^{17}/\mathrm{cm}^3\text{–}9.6 \times 10^{20}/\mathrm{cm}^3$. From the mobility data, it is also evident that there is a large variation in the level of disorder of these films. In this paper, we investigate various phonon modes, with two very different Raman excitation energy under similar experimental setup, of the InN thin film samples having such an extensive variation in the carrier density and level of disorder.

The Raman spectra of InN films were recorded in backscattering geometry $[z(x,\cdot)\bar{z}]$ using a Renishaw micro-Raman system with visible (514.5 nm=2.41 eV) and near infrared (785 nm=1.58 eV) laser excitation lines as shown in Figs. 1(a) and 1(b), respectively. The scattering geometry used in the experiments can only excite E_2 (high) and A_1(LO) phonon modes of InN. In general, the Raman spectra of MBE samples show sharp phonon modes at the expected energies of the E_2 (high) 490 cm^{-1} and $A_1(\mathrm{LO}) \sim 587\ \mathrm{cm}^{-1}$ modes as shown by hatched sphere and solid sphere, respectively. The PSMBE samples show similar values for these phonon frequencies but the peaks are broad and the band shape is strongly dependent on the carrier concentration. The films grown with two different growth techniques are of different thickness, doping levels, and structural quality. It seems from Figs. 1(a) and 1(b) that these parameters strongly influence the Raman spectra of the films. It is interesting to note that the energy absorption edge of 1.5–1.9 eV, in PSMBE samples, is closer to the excitation energy (2.41 eV or 1.58 eV) compared to 0.6–0.7 eV in MBE samples. This may lead to near-resonance enhancement of the Raman signal similar to the observations in AlN, InAlN, GaN, and related nitride films.[30] Furthermore, the A_1 (TO) mode $\sim 445\ \mathrm{cm}^{-1}$ which is forbidden in this scattering geometry is also observed in all the PSMBE samples, perhaps due to their polycrystalline nature. Due to the penetration of near-infrared energy into the sapphire substrate, in the case of relatively thinner films (thickness ~0.5 μm) grown by the PSMBE technique, we also observed sapphire peaks as marked by an asterisk (*) in Fig. 1(b).

The excitation source energy in the Raman experiment has a very strong influence on the spectral intensity of the modes as well as on the excitation of the new modes which otherwise could be absent. In Fig. 1(b) one observes a strong enhancement in the intensity of the LO-phonon-like mode in comparison to the E_2(high) mode, particularly in MBE samples where n_e varies from $6.7 \times 10^{17}/\mathrm{cm}^3$ to $1.2 \times 10^{19}/\mathrm{cm}^3$. There is the appearance of an additional broad peak around $\sim 540\ \mathrm{cm}^{-1}$ which is absent with 514.5 nm excitation energy. This peak gains intensity with increasing carrier concentration and its energy value suggests that it a B_1 (high) mode which also has been observed by others.[31]

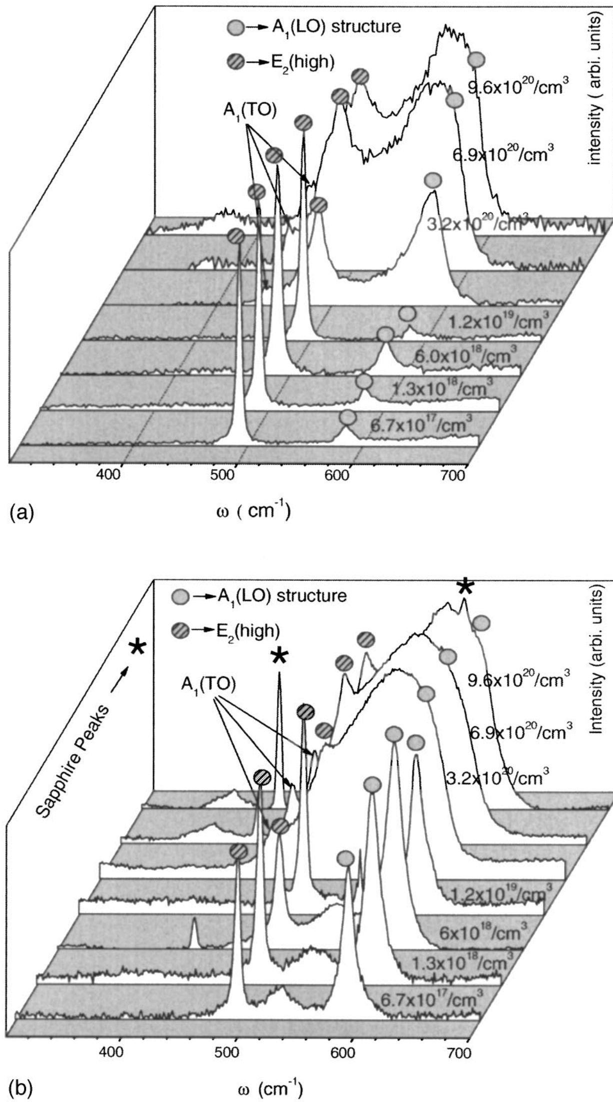

FIG. 1. Raman spectra of InN thin films excited with (a) 514.5 nm and (b) 785 nm laser wavelengths for various values of electron density.

III. THEORETICAL DISCUSSION OF THE LO-PHONON-LIKE STRUCTURE

In this paper we discuss the spectral lines of the coupled modes formed by the interaction of electronic excitations and LO phonons in InN semiconductors by employing a wave-vector-dependent dielectric function $\varepsilon(q,\omega)$. The total dielectric function of a coupled electron-phonon system can be written as

$$\varepsilon(q,\omega) = \varepsilon_{ph}(q,\omega) + \varepsilon_{el}(q,\omega), \tag{1}$$

where $\varepsilon_{ph}(q,\omega)$ and $\varepsilon_{el}(q,\omega)$ are the lattice (phonon) and electron dielectric functions, respectively. The phonon[32–34] contribution is given by

$$\varepsilon_{ph}(q,\omega) = \frac{(\omega_{LO}^2 - \omega_{TO}^2)}{(\omega_{TO}^2 - \omega^2 - i\omega\gamma)}. \tag{2}$$

Here, ω_{LO}/γ and ω_{TO} are the unscreened LO-phonon resonant-frequency and -damping[33] parameters and TO-phonon frequency, respectively. We use the energy of unscreened $\omega_{LO}=590\ \mathrm{cm}^{-1}$ from theoretical calculations on InN films[15–17] and ω_{TO} is determined from Lyddane-Sachs-Teller relation $\omega_{TO}=\omega_{LO}\sqrt{\varepsilon_\infty/\varepsilon_0}$, while the anharmonicity parameter γ is taken as a variable parameter to fit the calculated width of the LO-phonon structure with the experimental one. For the phonons dielectric function, we took a q-independent dispersion because of the smaller LO-TO splitting, $(\omega_{LO}-\omega_{TO})/\omega_{TO}$ in InN semiconductors. The electronic counterpart in the random phase approximation for damped electrons is given by

$$\varepsilon_{el}(q,\omega) = \varepsilon_\infty + V(q)\chi(q,\omega + i\Gamma). \tag{3}$$

Here, ε_∞ is the high-frequency dielectric constant of the material and we use[10] $\varepsilon_\infty=6.7$ and $\varepsilon_0=9.5$ in our calculations. $V(q)=4\pi e^2/q^2$ is Fourier transform of the Coulomb interaction potential between the electrons. Collisional damping effects of the electrons are calculated through the Mermin's description[35] for the susceptibility function by employing particle-conserving expression

$$\chi(q,\omega + i\Gamma) = \frac{\chi^0(q,\omega+i\Gamma)}{1 - \dfrac{i\Gamma}{\omega+i\Gamma}\left[1 - \dfrac{\chi^0(q,\omega+i\Gamma)}{\chi^0(q)}\right]}. \tag{4}$$

Here, the temperature-dependent Lindhard function[36] is given by

$$\chi^0(q,\omega+i\Gamma) = \sum_{k,\sigma} f(k,T)\left[\frac{1}{E_{k+q}-E_k+\hbar\omega+i\Gamma} + \frac{1}{E_{k+q}-E_k-\hbar\omega-i\Gamma}\right], \tag{5}$$

where $f(k,T)$ is the Fermi-Dirac distribution function, E_k is the electron dispersion for wave vector $\mathbf{k}$, and σ is the electron spin index. The use of the Lindhard function $\chi^0(q,\omega+i\Gamma)$ instead of $\chi(q,\omega+i\Gamma)$ defined in Eq. (4) violates particle conservation[35] and the effect of this violation will be directly reflected in the shift of the onset of Landau damping[36] which thus leads to a shift in the peak positions and also a change in the spectral intensity. The carrier density in some of the samples we investigated is quite high, $\geqslant 10^{20}/\mathrm{cm}^3$, so the electron dispersion deviates significantly from the parabolic behavior. We employed in our calculations a nonparabolic dispersion[11] given by

$$E(k) = \frac{\hbar^2k^2}{2m^*} = E_g + \frac{\hbar^2k^2}{2m_e^{\ 0}} + \frac{1}{2}\left(\left[E_g^{\ 2} + 4E_p\frac{\hbar^2k^2}{2m_e^{\ 0}}\right]^{1/2} - E_g\right), \tag{6}$$

which correctly takes into account the electron's effective mass ($m_e^{\ 0}$ is the bare electron mass) variation with electron density. At smaller electron densities, the nonparabolic effects can also not be neglected for larger values of the wave vector $\mathbf{k}$. The best fit for the effective mass is obtained by varying the parameter E_p from 7.5 eV to 15 eV depending on the value of the Fermi energy.[11] However, in our calculations we have taken a fixed value of $E_p=10$ eV. In what follows, in equations only, we express all the energy terms (E_g, E_p,

ω_p and $\hbar\omega$) and damping parameters (Γ and γ) in terms of Fermi energy $E_F=\hbar^2 k_F{}^2/2m_e{}^*$ and wave vectors ($\mathbf{k}$ and $\mathbf{q}$) in terms of Fermi wave vector k_F. Defining variables $\varepsilon=k^2$ and $x=\cos(\theta)=\hat{k}\hat{q}$ (here θ is the angle between wave vector $\mathbf{k}$ and $\mathbf{q}$), the phase-space summation in Eq. (5) after using Eq. (6) can be rewritten as

$$\chi^0(q,\omega+i\Gamma)=\frac{3}{2}\frac{n_e}{E_F}\frac{m^*}{m_0}\int_0^\infty d\varepsilon f(E(\varepsilon)-\mu,T)\sqrt{E(\varepsilon)}\times\left[1+\frac{E_p}{\sqrt{E_g{}^2+4E_p\varepsilon}}\right]\times\int_{-1}^{1}dx\left[\frac{1}{\Delta(q,\varepsilon,x)+\hbar\omega+i\Gamma}+\frac{1}{\Delta(q,\varepsilon,x)-\hbar\omega-i\Gamma}\right], \quad (7)$$

where

$$E(\varepsilon)=E_g+\varepsilon\frac{m^*}{m_0}+\frac{1}{2}\left(\sqrt{E_g^2+4E_p\frac{m^*}{m_0}\varepsilon}-E_g\right)$$

and the intraband excitation energy $\Delta(q,\varepsilon,x)$ of an electron in a nonparabolic conduction band according to Eq. (6) can be written as

$$\Delta(q,\varepsilon,x)=\frac{m^*}{m_0}(q^2+2qx\sqrt{\varepsilon})+\frac{1}{2}\left[E_g^2+4E_p\frac{m^*}{m_0}(\varepsilon+q^2+2qx\sqrt{\varepsilon})\right]^{1/2}-\frac{1}{2}\left[E_g^2+4E_p\frac{m^*}{m_o}\varepsilon\right]^{1/2}. \quad (8)$$

For a given electron density, a nonparabolic dispersion affects the highest filled energy level of an electron because of the deviation of its energy-dispersion curvature compared to the parabolic dispersion. So the determination of the chemical potential, which depends on the energy dispersion and temperature, becomes important. Particularly at low electron densities, temperature strongly influences the value of chemical potential. So in the Fermi-Dirac distribution function, which modifies the value of the plasmon mode of the system and thus changes the energies of the coupled modes, it becomes important to employ an appropriate chemical potential in the calculations. From the energy-dispersion relation given by Eq. (6), the temperature and n_e-dependent chemical potential is determined by a nonlinear equation

$$n_e=\frac{k_F{}^3}{2\pi^2}\int_0^\infty d\varepsilon\sqrt{E(\varepsilon)}\left[1+\frac{E_p}{\sqrt{E_g{}^2+4E_p\varepsilon}}\right]f(E(\varepsilon)-\mu,T). \quad (9)$$

A. Landau damping modes at low carrier density

The low carrier densities here we mean that the plasmon energy is smaller than the LO-phonon energy. In a degenerate semiconductor material, the value of carrier density determines the energy scales of an electron interaction with various other electric-field sources of the system. For example, the value of plasmon energy relative to the LO-phonon energy determines the interaction strength between the two modes of the system. Similarly, the Fermi energy level decides the electron scattering mechanisms[37] and thus affects the mobility and other electrical transport properties of the system. For a given electron density, we determine the chemical potential at room temperature from Eq. (9) which we then used to evaluate the electron dielectric function Eq. (3). Figure 2(a) shows Im $\varepsilon(q,\omega)^{-1}$ for our lowest-electron-density $n_e=6.7\times10^{17}/\text{cm}^3$ sample, calculated from Eq. (1), at different q values. In order to see a weak EHP's spectrum in the presence of high-intensity coupled modes, we choose a small value of the collisional damping parameter, $\Gamma=16\ \text{cm}^{-1}$, while the phonon damping parameter γ is adjusted to fit the calculated width of the LO-phonon-like structure with the experimental structure. Values of both these parameters strongly influence the spectral features—intensity, width, and peak positions of the coupled modes, etc.—of the Raman spectra.[27] At this low value of carrier density $n_e=6.7\times10^{17}/\text{cm}^3$, the Fermi energy ($E_F=0.056$ eV) is comparable with the thermal energy ($k_BT=0.025$ eV), so thermal broadening effects can significantly dampen the spectrum, particularly the small-wave-vector single-particle excitation spectrum.

For small values of $\mathbf{q}$, one expects three distinct excitation spectra in the system if the electron collisional and phonon dampings are small: (1) the $\mathbf{q}$-dependent EHP excitation spectrum, (2) the lower-energy coupled mode and (3) the higher-energy coupled mode. These features are very generic of the electron-phonon system and expected to exist at all values of carrier density but with very different intensities. The coupled modes for InN semiconductors are not experimentally very well understood yet, as they have been found in a few samples with high carrier densities.[23,38] The intensity of the EHP excitation spectrum is strongly influenced by the collisional damping of the electrons and for small damping the well-defined upper edge of this broad spectrum propagates gradually with increasing values of $\mathbf{q}$. At a small wave vector $\mathbf{q}=5.2\times10^5\ \text{cm}^{-1}$, most of the spectral strength is exhausted by the coupled modes and only a small fraction of the intensity is contributed by the EHP excitations. At smaller values of $\mathbf{q}$, the LO phonon interacts with the electronic subsystem mainly via two channels—EHP excitations and plasmons. Interaction with EHP's is much weaker owing to the weaker Coulomb potential of the EHP excitations. So the LO phonon mainly interacts with the plasmon and the resulting coupled modes have energies similar to that obtained by the interaction with the long-wavelength plasmon. In Fig. 2(a), one clearly observes the Landau damping of the lower-energy coupled mode followed by the Landau damping of the higher-energy coupled mode as $\mathbf{q}$ values are increased. Once both the coupled modes of the system are damped, the LO structure begins to appear from the region of damped higher-energy coupled mode which eventually becomes a well-defined structure at larger values of $\mathbf{q}$.

The character of the each coupled mode strongly depends on the value of plasmon energy relative to LO-phonon energy. At $n_e=6.7\times10^{17}/\text{cm}^3$, the plasmon energy

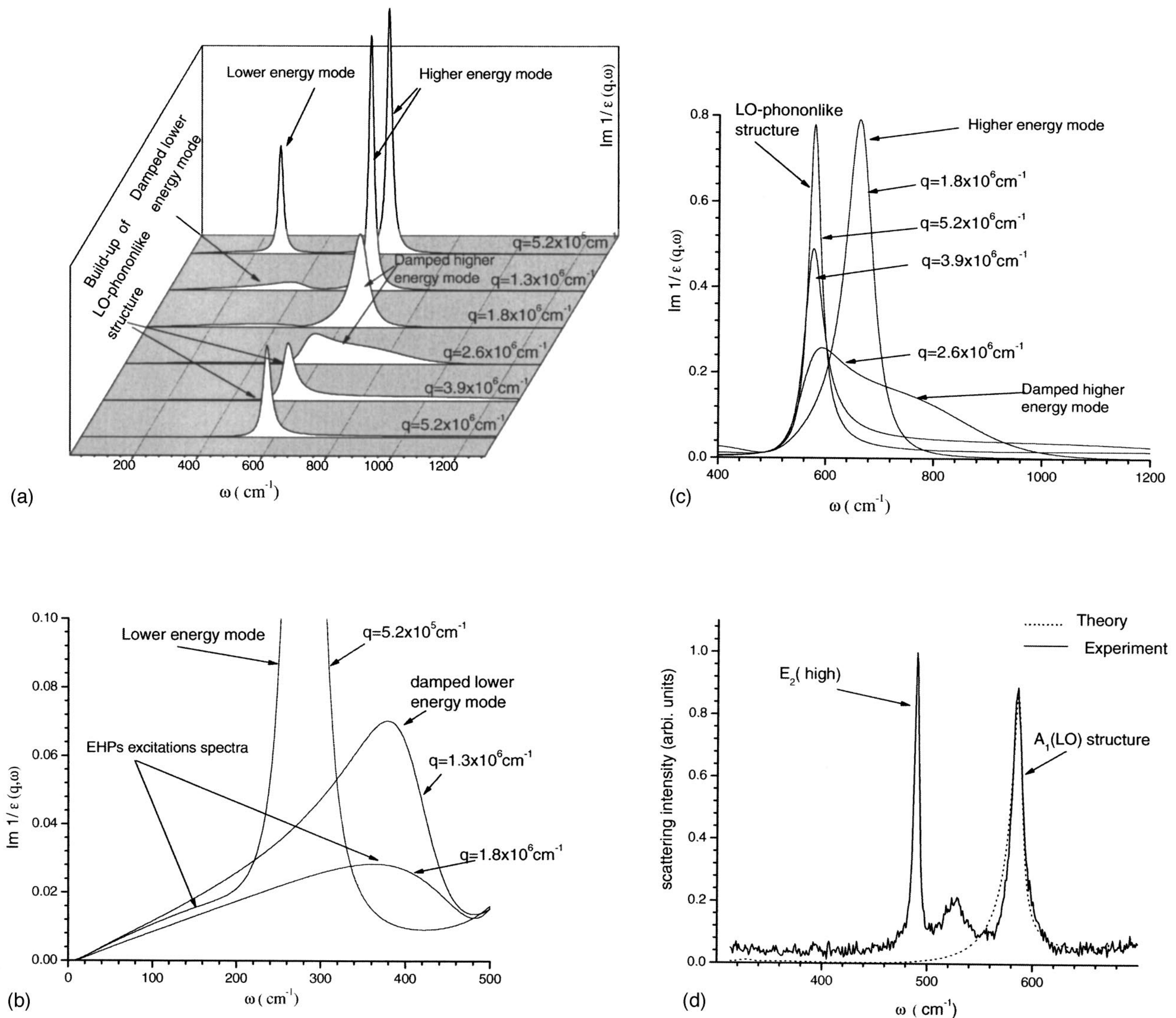

FIG. 2. (a) Spectral features of the coupled modes plotted as a function of ω (cm^{-1}) for a $n_e=6.7\times10^{17}$ cm^{-3} sample at different wave vectors, labeled against each curve. Both coupled modes are clearly observed for smaller values of **q**. (b) and (c) The spectral intensities of the lower- and higher-energy coupled modes plotted as a function of **q**, and (d) the experimental spectra (solid curve) of the LO-phonon-like structure and theoretical fitting (dotted curve) for it.

$\omega_p=424$ cm^{-1} is smaller than the LO-phonon energy, so the character of the lower-energy coupled mode is plasmon like, which means that its energy varies with **q**, as seen in Fig. 2(b). On the other hand, the higher-energy coupled mode [Fig. 2(c)] is phonon like and almost dispersionless [Fig. 2(a)]. At a small value of $\mathbf{q}=5.2\times10^5$ cm^{-1}, the upper edge of the EHP spectrum is away from the resonance frequency of the lower-energy coupled mode, so there is not much interaction between EHP excitations and the coupled modes. As **q** increases further, the upper edge of the EHP spectrum begins to enter into the lower-energy coupled spectrum and this energy overlap initiates the Landau damping process of the lower-energy coupled mode. At $\mathbf{q}=1.3\times10^6$ cm^{-1}, the lower-energy mode becomes Landau damped, leading to a broad spectrum which is a mixture of the damped coupled mode and EHP excitations. At a larger value of $\mathbf{q}=1.8\times10^6$ cm^{-1}, the spectrum becomes very broad across the range where the lower-energy coupled mode existed. With a further increase in the **q** value, the EHP spectrum approaches the higher-energy coupled mode. Figure 2(c) shows the Landau damping of the higher-energy coupled and the emergence of the LO structure, which begins to form a well-defined peak near the LO-phonon energy. Two interesting features of the Landau-damped higher-energy coupled mode are (1) an emergence of a peak structure near the undamped mode energy and (2) a spectral asymmetry on the higher-energy side of this structure due to the broad background spectrum of the EHP excitations. After Landau damping of the higher-energy mode, there is no coupled mode left in the system.

The cutoff wave vector $\mathbf{q}_c$ for this almost-dispersionless higher-energy coupled mode can be determined from $E(k+q)-E(k)=\omega_{n_e}^H$, here $\omega_{n_e}^H$ is the energy of the higher-energy coupled mode. $\omega_{n_e}^H$ can also be estimated from the higher-energy zero of the equation $\varepsilon'(q,\omega)=0$; here, $\varepsilon'(q,\omega)$ is the real part of $\varepsilon(q,\omega)$ defined by Eq. (1). Using Eq. (6), $E(k$

$+q)-E(k)=\omega_{n_e}^H$ can be solved for $\mathbf{q}_c$ by defining $b=(E_g^2+4E_p m^*/m_0)^{1/2}+E_p+2\omega_{n_e}^H$ and

$$c=\left[(\omega_{n_e}^H)^2+\omega_{n_e}^H\left(E_g^2+4E_p\frac{m^*}{m_0}\right)^{1/2}\right].$$

We finally get

$$q_c=-1+\left[1+\frac{1}{2}\frac{m_0}{m^*}[b-\sqrt{b^2-4c}]\right]^{1/2}. \qquad (10)$$

In deriving Eq. (10), it is assumed that the energy $\omega_{n_e}^H$ of the higher-energy coupled mode is dispersionless. Physically, this cutoff wave vector for the higher-energy coupled mode also defines the point at which the new peak structure begins to form on the lower-energy side of the higher-energy coupled mode which at larger values of **q** develops into a sharp peak structure. The **q**-dependent behavior of the higher-energy coupled mode changes with electron density as we discuss in the subsequent sections. With increasing values of carrier density, this mode begins to develop a **q**-dependent dispersion, and at higher electron density where $\omega_p>\omega_{LO}$, the mode becomes plasmon like and its energy varies appreciably with **q**. So the above relation, Eq. (10), for the cutoff wave vector is only valid when $\omega_p<\omega_{LO}$.

Figure 2(d) shows the experimental Raman spectrum (solid curve) for our lowest electron density $n_e=6.7\times10^{17}/\mathrm{cm}^3$ sample along with our calculated values shown by the dotted curve. The **q**-nonconserving mechanism in the Raman scattering intensity is taken into account by folding a **q**-conserving response function[29,39]

$$L(q,\omega)=q^2S(\omega)\mathrm{Im}\left\{\frac{-1}{\varepsilon(q,\omega)}\right\}, \qquad (11)$$

with a Yukawa-type impurity potential weight function[29,40]

$$F(q)=\left(\frac{4\pi}{q^2+q_{FT}^2}\right)^2, \qquad (12)$$

where the function $S(\omega)$ depends on the scattering mechanism.[29] The weighted scattering cross section for the Raman scattering processes for **q** up to $q_{FT}=\omega_p\sqrt{3m^*/(2E_Fk_F^2)}$ (q_{FT} is Fermi-Thomas screening wave vector expressed in units of the Fermi wave vector k_F) is given by

$$I(\omega)=\int_0^{q_{\max}}dqF(q)L(q,\omega). \qquad (13)$$

Here $q_{\max}$ is the cutoff wave vector chosen in such a way that convergent results for $I(\omega)$ are obtained and we find that $q_{\max}=5.0q_{FT}$ was sufficient to obtain a convergent result. For the scattering mechanism[29] which is incorporated by the function $S(\omega)$, the best fit of Eq. (13) to the experimental intensity is obtained by "forbidden" impurity-induced Fröhlich mechanism. While calculating Im $\varepsilon(q,\omega)^{-1}$, two parameters are varied: The first is Γ; although this parameter does not much affect the spectral features of the LO-phonon-like structure, we estimate it from the optical reflectance measurements data for the corresponding carrier density using Drude model for the dielectric function. The second is γ, which determines the width of the LO-phonon-like structure. For this particular case, the values of $\Gamma=140\ \mathrm{cm}^{-1}$ and $\gamma=6.0\ \mathrm{cm}^{-1}$.

B. Landau damping of modes at high carrier density

In Fig. 3(a) we show Im $\varepsilon(q,\omega)^{-1}$ calculated for $n_e=9.6\times10^{20}/\mathrm{cm}^3$ for different values of **q** shown by a label against each curve. In order to see various modes at such a high density, we use $\Gamma=300\ \mathrm{cm}^{-1}$ and $\gamma=20\ \mathrm{cm}^{-1}$. At this value of electron density, the energy scales ($E_F=10\,220\ \mathrm{cm}^{-1}$ and $\omega_p=6775\ \mathrm{cm}^{-1}$) of the degenerate electron gas are much higher than the phonon system—e.g., ω_{LO} energy. Hence, the interaction between the plasmon and phonon modes is quite weak, and as a result the higher-energy coupled mode is plasmon like, while the lower-energy coupled mode is phonon like. Because of the stronger electron degeneracy, the thermal broadening effects on the spectrum are not significant at this value of density. The plasmonlike higher-energy coupled mode shows significant dispersion with increasing values **q**. At $\mathbf{q}=9.2\times10^6\ \mathrm{cm}^{-1}$, the EHP excitation spectrum can be seen approaching this mode from the lower-energy side, which will Landau-damp this coupled mode at a larger value of **q**. Because of the stronger intensity of this mode, the lower-energy mode is not visible on this intensity scale. However, at $\mathbf{q}=9.2\times10^6\ \mathrm{cm}^{-1}$ a peak structure begins to appear on the lower-energy side of the spectrum which transforms into a sharp peak at $\mathbf{q}=3.1\times10^7\ \mathrm{cm}^{-1}$.

Figure 3(b) shows the behavior of the lower-energy coupled mode as a function of **q**. The plasmon like mode is very intense at this value of density, so in order to see the EHP spectrum and the lower-energy coupled mode, we calculated Im $\varepsilon(q,\omega)^{-1}$ at a smaller value of damping parameter ($\Gamma=30\ \mathrm{cm}^{-1}$). With increasing values of **q**, the EHP's quickly damp this mode and at $\mathbf{q}=1.5\times10^6\ \mathrm{cm}^{-1}$ a structure begins to form at the energy of the lower-energy coupled mode. Since the lower-energy mode shows negligible dispersion with increasing **q**, one can use Eq. (10), after replacing $\omega_{n_e}^H$ with ω_{TO} energy, to determine the critical wave vector at which this mode becomes Landau damped.

In Fig. 3(c), the plasmonlike higher-energy coupled mode shows strong energy dispersion with increasing wave vector **q**, which eventually becomes Landau damped around $\mathbf{q}=1.6\times10^7\ \mathrm{cm}^{-1}$. After damping of the higher-energy mode, the structure which emerges near the lower-energy coupled mode [Fig. 3(b)] starts building its intensity with increasing wave vector. In Fig. 3(d) we show the buildup and dispersion of the LO-phonon-like structure at this high value of electron density.

In Fig. 3(e), we plot the experimental Raman spectrum (solid curve) for our highest-density sample, $n_e=9.6\times10^{20}/\mathrm{cm}^3$, and the corresponding theoretical spectrum (dotted curve) calculated using Eq. (13) with a forbidden impurity-induced Fröhlich mechanism. The best fit for the intensity is obtained by using for $\gamma\approx25\ \mathrm{cm}^{-1}$ in Eq. (2). The experimental data show a broad spectrum in the energy range from 470 to 640 cm^{-1} which includes LO-phonon-like structure, E_2(high), and also A_1(TO) modes. In addition to these,

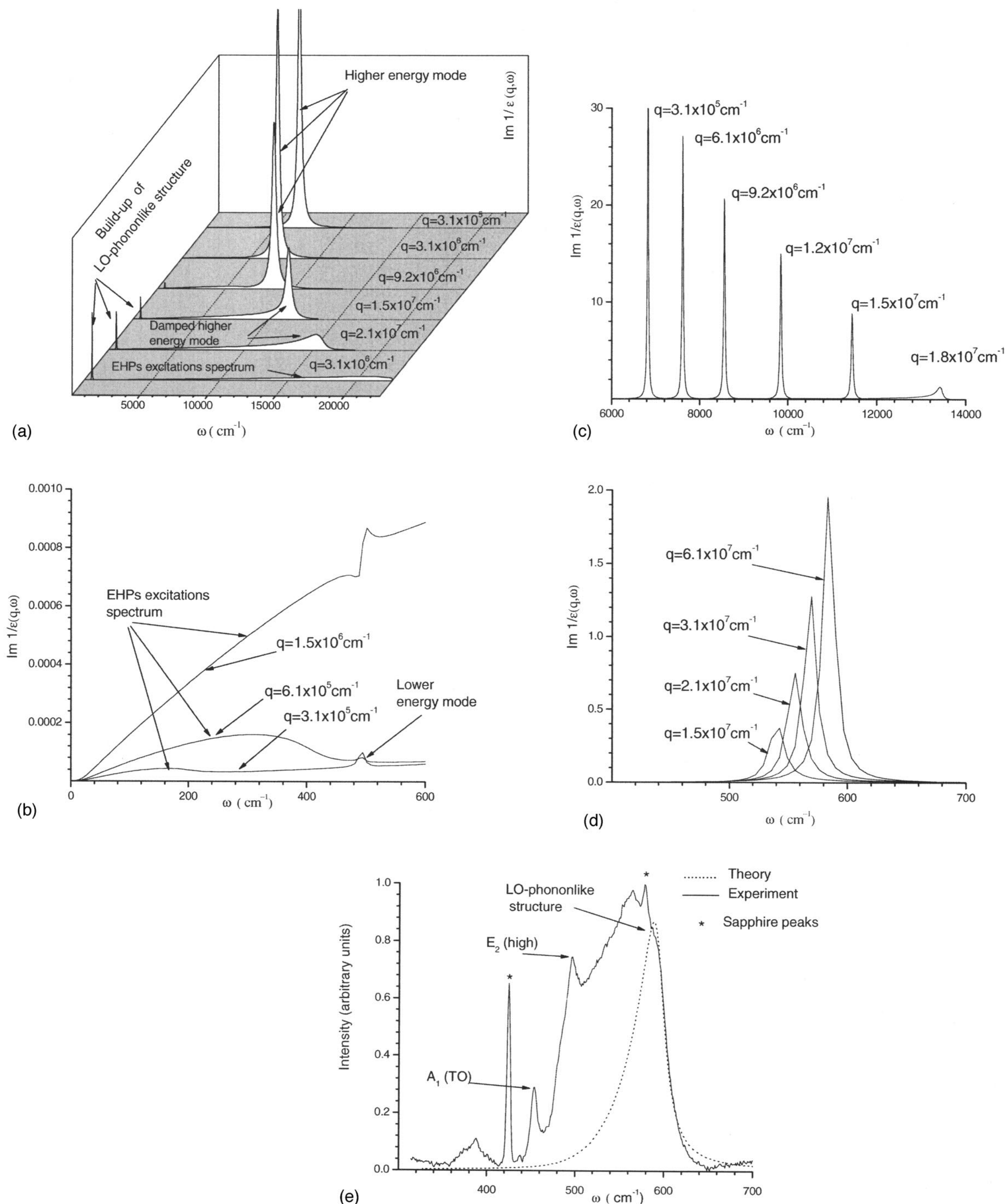

FIG. 3. (a) Spectral features of the coupled modes plotted as a function of ω (cm^{-1}) for a $n_e=9.6\times10^{20}$ cm^3 sample at different wave vectors, labeled against each curve. Both coupled modes are clearly observed for smaller values of **q**. (b) and (c) The spectral intensities of the lower- and higher-energy coupled modes are plotted as a function of **q**. (d) Buildup and dispersion of LO-phonon-like structure, and (e) the experimental spectra (solid curve) of the LO-phonon-like structure and theoretical fitting (dotted curve) for it.

the sapphire peak at 578 cm^{-1} is also observed. Our high-electron-density samples are found to be polycrystalline with much larger disorder than the low-density samples, which can lead to a substantial off c-axis scattering. It is well known that the presence of a disorder breaks the translational symmetry of crystal, which can lead to the activation of forbidden Raman modes of the system. A_1(TO) is not allowed in the backscattering geometry configuration of c-axis-oriented films. Similarly B_1(high) is another forbidden mode whose energy[31,41] is around 540 cm^{-1} which lies in the middle of E_2(high) and A_1(LO) modes. Activation of such a mode [B_1(high)] when superimposed with E_2(high) and A_1(LO) modes including the sapphire peak can create a very broad spectral intensity around B_1(high) mode. At a low

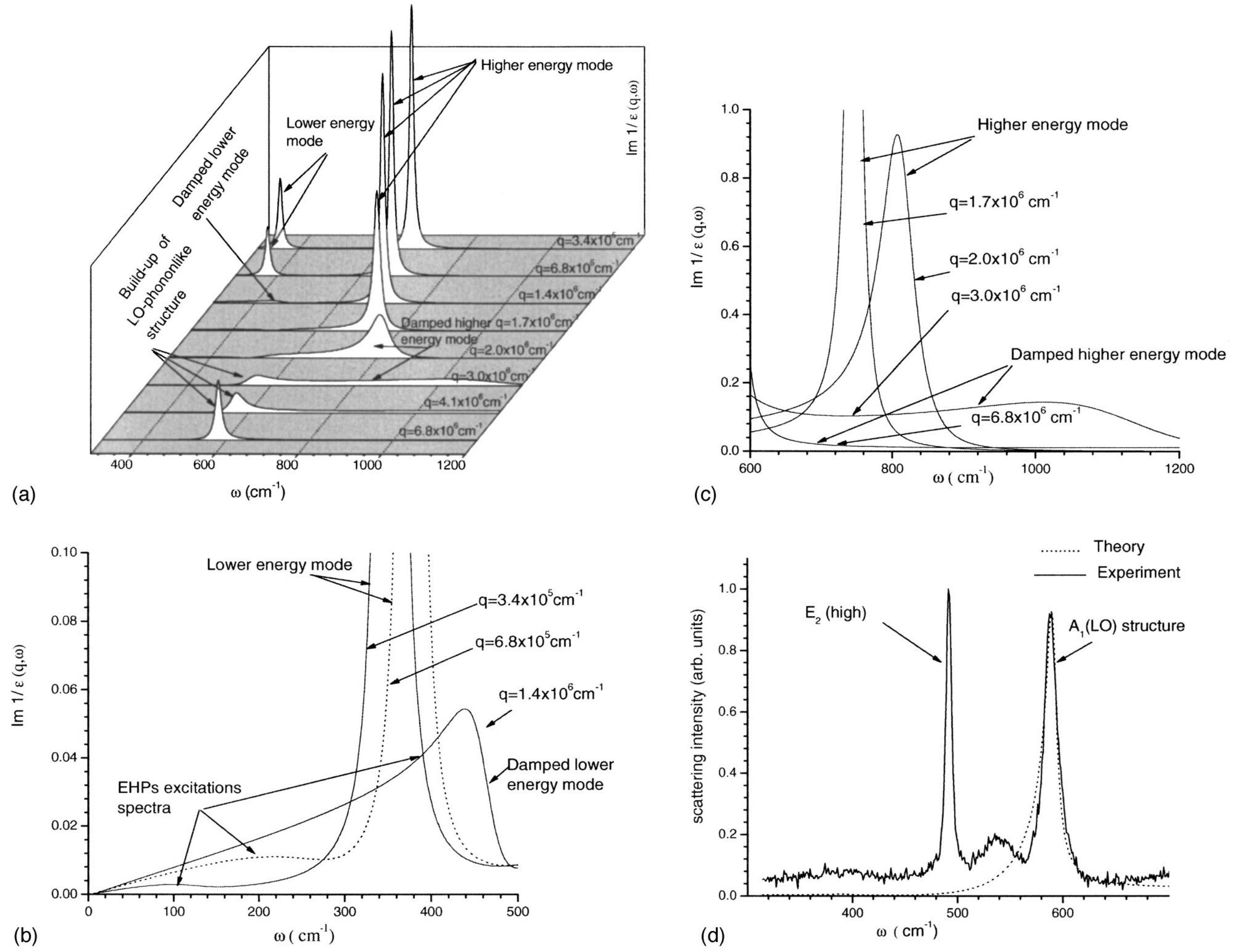

FIG. 4. (a) Spectral features of the coupled modes plotted as a function of ω (cm^{-1}) for a $n_e = 1.3 \times 10^{18}$ cm^{-3} sample at different wave vectors, labeled against each curve. (b) and (c) The spectral intensities of the lower- and higher-energy coupled modes are plotted as a function of $\mathbf{q}$, and (d) the experimental spectra (solid curve) of the LO-phonon-like structure and theoretical fitting (dotted curve) for it.

electron density, Fig. 2(d), the theoretical calculations of the Raman spectral intensity for the A_1(LO) mode are in good agreement with the experimental results; however, at higher electron densities, the comparison is tentative, but cannot be completely satisfactory.

C. Landau damping of modes at intermediate carrier density

When the electron density is such that the plasmon mode's energy is close to the LO-phonon energy, the energy exchange between the two modes becomes very efficient. Both the coupled modes in this case will have a mixed character of phonon and plasmon. Figure 4(a) shows Im $\varepsilon(q,\omega)^{-1}$ calculated for $n_e = 1.3 \times 10^{18}/\mathrm{cm}^3$ at different values of $\mathbf{q}$ as shown by the labels. In this case the values of damping parameters are $\Gamma = 173$ cm^{-1} and $\gamma = 12$ cm^{-1}. At this value of electron density, the plasmon energy $\omega_{\mathrm{p}} = 539$ cm^{-1} is close to the A_1(LO) phonon energy. It is interesting to contrast the behavior and dispersion of the coupled modes at this intermediate electron density with the low- and high-density cases. In Figs. 4(b) and 4(c) we show the Landau damping of the lower- and higher-energy coupled modes, respectively, and both the coupled modes show appreciable energy dispersion with $\mathbf{q}$. LO-phonon-like structure emerges from in between the two coupled modes bands. The experimental spectrum (solid curve) for $n_e = 1.3 \times 10^{18}/\mathrm{cm}^3$ along with the theoretical values (dotted line) calculated using Eq. (13) with the forbidden impurity-induced Fröhlich mechanism and $\gamma = 7$ cm^{-1} and $\Gamma = 173$ cm^{-1} are shown in Fig. 4(d).

IV. EMERGENCE OF THE LO-PHONON-LIKE STRUCTURE

We observed that in order to nullify the effects of a strong plasmon waves electric field on the LO-phonon mode, the plasmon needs to be Landau damped. The electronic subsystem is then left only with the incoherent excitations due to the EHP's and this state can only be achieved by exciting the electronic subsystem with $\mathbf{q}$ larger than the cutoff wave vector. In this situation, the LO phonon is left to interact with a weak electric field of the EHP excitations whose spectral strength is broadly distributed in intensity over a wide range of energy. Energetically those EHP excitations, which are resonant with the LO-phonon energy, interact strongly with

phonons and give rise to a buildup of the structure as we clearly observed in Figs. 2(a) and 4(a). A signature of this mode begins to appear with an asymmetric spectral feature on the lower-energy side of the LO-phonon energy even when **q** is less than the cutoff wave vector of the higher-energy coupled mode and becomes quite prominent when **q** becomes larger than the cutoff wave vector. At this stage the spectral strength of the coupled mode is significantly smeared out and this new mode emerges out of the EHP spectrum.

It is expected that if both polar-A_1(LO) and nonpolar-E_2(high) modes of the system are excited then they will interact in a qualitative different way with conduction band electrons. This interaction will modify the modes energy and their widths. Figures 1(a) and 1(b) show how the energies of the polar LO-phonon-like structure and nonpolar-E_2(high) modes are affected due to the variation of the electron density. Due to the nonpolar character of the E_2(high) mode, there is no interaction of this mode with the conduction-band electrons and as expected the energy and broadening of this mode remain unaffected as electron density is varied. On the other hand, the A_1(LO) mode strongly interacts with the conduction-band electrons and the magnitude of this interaction depends on the value of electron density. The energy of the observed LO-phonon-like structure [Figs. 1(a) and 1(b)] is found to increase from 587 to 591 cm^{-1} as n_e is varied from $6.7\times 1017/cm^3$ to $1.2\times 10^{19}/cm^3$. In this range of electron density, these values agree with other experimental results. At higher values of n_e the correlation between the peak position and electron density could not be established due to the activation of other forbidden modes. Note that the above slow increase in the energy of the LO-phonon-like structure is not consistent with the rapid variation of the coupled modes energy with carrier density.

V. SUMMARY

In this paper we have discussed the LO-phonon-like structure of InN films for a wide range of electron density. The experimentally observed structure is investigated by studying a wave-vector-dependent dielectric function of an electron–LO-phonon system. It is found that when the higher-energy coupled mode becomes Landau damp, the LO phonon interacts with a weaker field of the incoherent excitations of the EHPs. This interaction creates a structure which begins to emerge out of the EHP spectrum when **q** becomes larger than the cutoff wave vector of the higher-energy coupled mode and becomes more mature at larger values of **q**. Experimentally it is found that the energy of this structure depends on the electron density and found to increase with it.

ACKNOWLEDGMENTS

This work is supported by NSF-IGERT-DGE Grant No. 9870720 and by the Center for Smart Sensors and Integrated Microsystems at Wayne Sate University, Detroit.

*Electronic address: jagdish@wayne.edu

[1] V. Yu Davydov *et al.*, Phys. Status Solidi B **229**, R1 (2002); V. Yu. Davydov *et al.*, *ibid.* **230**, R4 (2002).

[2] A. Kasic, M. Schubert, Y. Saito, Y. Nanishi, and G. Wagner, Phys. Rev. B **65**, 115206 (2002).

[3] J. Wu, W. Walukiewicz, K. M. Yu, J. W. Ager III, E. E. Haller, H. Lu, W. J. Schaff, Y. Saito, and Y. Nanishi, Appl. Phys. Lett. **80**, 3967 (2002).

[4] S. C. Jain, M. Willander, J. Narayan, and R. Van Overstraeten, J. Appl. Phys. **87**, 965 (2000).

[5] T. Matsuoka, H. Okamoto, M. Nakao, H. Harima, and E. Kurimoto, Appl. Phys. Lett. **81**, 1246 (2002).

[6] D. C. Look, H. Lu, W. J. Schaff, J. Jansinski, and Z. Liliental-Weber, Appl. Phys. Lett. **80**, 258 (2002); D. W. Jenkins and J. D. Dow, Phys. Rev. B **39**, 3317 (1989).

[7] K. Ikuta, Y. Inoue, and O. Takai, Thin Solid Films **334**, 49 (1998).

[8] T. L. Tansley and C. P. Foley, J. Appl. Phys. **59**, 3241 (1986); **60**, 2092 (1986).

[9] T. V. Shubina, S. V. Ivanov, V. N. Jmerik, D. D. Solnyshkov, V. A. Vekshin, P. S. Kop'ev, A. Vasson, J. Leymarie, A. Kavokin, H. Amano, K. Shimono, A. Kasic, and B. Monemar, Phys. Rev. Lett. **92**, 117407 (2004).

[10] D. B. Haddad, J. S. Thakur, V. M. Naik, G. W. Auner, R. Naik, and L. E. Wenger, in *GaN and Related Alloys*, edited by C. Wetzel, E. T. Yu, J. S. Speck, A. Rizzi, and Y. Arakawa, MRS Symposia Proceedings No. 743 (Materials Research Society, Warrendale, PA, 2003), p. L11.22.

[11] J. Wu, W. Walukiewicz, W. Shan, K. M. Yu, J. W. Ager III, E. E. Haller, H. Lu, and W. J. Schaff, Phys. Rev. B **66**, 201403 (2002); H. Lu, W. J. Schaff, H. Hwang, H. Wu, G. Koley, and L. F. Eastman, Appl. Phys. Lett. **79**, 1489 (2001).

[12] K. Lawniczak-Jablonska, T. Suski, I. Gorczyca, N. E. Christensen, K. E. Attenkofer, R. C. C. Perera, E. M. Gullikson, J. H. Underwood, D. L. Edger, and Z. L. Weber, Phys. Rev. B **61**, 16 623 (2000).

[13] C. Persson, R. Ahuja, A. F. da Silva, and B. Johansson, J. Phys.: Condens. Matter **13**, 8945 (2001).

[14] F. Bechstedt and J. Furthmüller, J. Cryst. Growth **246**, 315 (2002).

[15] J. S. Dyck, K. Kim, S. Limpijumnong, W. R. L. Lambrecht, K. Kash, and J. C. Angus, Solid State Commun. **114**, 355 (2000).

[16] H. Grille, Ch. Schnittler, and F. Bechstedt, Phys. Rev. B **61**, 6091 (2000).

[17] C. Bungaro, K. Rapcewicz, and J. Bernholc, Phys. Rev. B **61**, 6720 (2000).

[18] T. Inushima, T. Shiraishi, and V. Yu. Davydov, Solid State Commun. **110**, 491 (1999).

[19] J. Aderhold, V. Yu. Davydov, F. Fedler, H. Klausing, D. Mistele, T. Rotter, O. Semchinova, J. Stemmer, and J. Graul, J. Cryst. Growth **222**, 701 (2001).

[20] B. B. Varga, Phys. Rev. **137**, A1896 (1965).

[21] This paper quotes a quite small value (572 cm^{-1}) for the A_1(LO) structure: J. S. Dyck, K. Kash, K. Kim, W. R. L. Lambrecht, C.

C. Hayman, A. Argoitia, M. T. Grossner, W. L. Zhou, and J. C. Angus, in *Nitride Semiconductors*, edited by F. A. Ponce, S. P. DenBaars, B. K. Meyer, S. Nakamura, and S. Strite, MRS Symposia Proceedings No. 482 (Materials Research Society, Pittsburgh, 1998), p. 549.

[22] This paper quotes a quite large value (596 cm^{-1}) for the A_1(LO) structure: H.-J. Kwon, Y.-H. Lee, O. Miki, H. Yamano, and A. Yoshida, Appl. Phys. Lett. **69**, 937 (1996).

[23] T. Inushima, V. V. Mamutin, V. A. Vekshin, S. V. Ivanov, T. Sakon, M. Motokawa, and S. Ohoya, J. Cryst. Growth **227-228**, 481 (2001).

[24] V. Yu. Davidov, A. A. Klochikhin, V. V. Emtsev, S. V. Ivanov, V. V. Vekshin, F. Bechstedt, J. Furthmuller, H. Harima, A. V. Mudryi, A. Hashimoto, A. Yamamoto, J. Aderhold, J. Graul, and E. E. Haller, Phys. Status Solidi B **230**, R4 (2002).

[25] A. Kawabata, J. Phys. Soc. Jpn. **30**, 68 (1971).

[26] M. Cardona, J. Phys. Soc. Jpn. **49**, Suppl. A, 23 (1980).

[27] J. S. Thakur, D. Haddad, V. Naik, R. Naik, and G. W. Auner, J. Appl. Phys. **95**, 4795 (2004).

[28] S. Katayama and K. Murase, J. Phys. Soc. Jpn. **42**, 886 (1977).

[29] For a review see, e.g., G. Abstreiter, M. Gardona, and A. Pinczuk, in *Light Scattering in Solids*, edited by M. Cardona and G. Güntherodt (Springer, Berlin, 1984), Vol. IV.

[30] V. M. Naik, W. H. Weber, D. Uy, D. Haddad, R. Naik, Y. V. Danylyuk, M. J. Lukitsch, G. W. Auner, and L. Rimai, Appl. Phys. Lett. **79**, 2019 (2001); H. Harima (Chap. 7) and J. Frandon *et al.* (Chap. 8), in *III-Nitride Semiconductors Optical Properties I*, edited by M. O. Monasreh and H. X. Jiang (Taylor & Francis, New York, 2002).

[31] A. G. Bhuiyan, T. Tanaka, A. Yamamoto, and A. Hashimoto, Phys. Status Solidi A **194**, 502 (2002).

[32] A. S. Barker, Jr. and R. Loudon, Rev. Mod. Phys. **44**, 18 (1972).

[33] C. R. Pidgeon, in *Handbook on Semiconductors*, edited by M. Balkanski (North-Holland, Amsterdam, 1980), Vol. 2, pp. 223–328.

[34] P. Y. Yu and M. Cardona, *Fundamentals of Semiconductors* (Springer, Berlin, 1999).

[35] N. D. Mermin, Phys. Rev. B **1**, 2362 (1970).

[36] D. Pines and P. Nozieres, *Theory of Quantum Liquids* (Benjamin, New York, 1966), Chap. 5.

[37] J. S. Thakur, L. Liu, and D. N. Neilson, Phys. Rev. B **59**, 7255 (1999); W. Gotze, Solid State Commun. **27**, 1393 (1978).

[38] V. Yu. Davidov, V. V. Emtsev, I. N. Goncharuk, A. N. Smirnov, V. D. Petrikov, V. V. Manutin, V. A. Vekshin, S. V. Ivanov, M. B. Smirnov, and T. Inushima, Appl. Phys. Lett. **75**, 3297 (1999).

[39] M. Ramsteiner, O. Brandt, and K. H. Ploog, Phys. Rev. B **58**, 1118 (1998).

[40] D. Olego and M. Cardona, Solid State Commun. **32**, 375 (1979).

[41] A. G. Bhuiyan, A. Hashimoto, and A. Yamamoto, J. Appl. Phys. **94**, 2779 (2004).